



HAL
open science

Comparison between Multi Line Transmission and Diverging Wave Imaging: assessment of image quality and motion estimation accuracy

Emilia Badescu, Damien Garcia, Philippe Joos, Adeline Bernard, Lionel Augeul, René Ferrera, Magalie Viallon, Lorena Petrusca, D. Friboulet, H. Liebgott

► To cite this version:

Emilia Badescu, Damien Garcia, Philippe Joos, Adeline Bernard, Lionel Augeul, et al.. Comparison between Multi Line Transmission and Diverging Wave Imaging: assessment of image quality and motion estimation accuracy. *IEEE Transactions on Ultrasonics, Ferroelectrics and Frequency Control*, 2019, 66 (10), pp.1560-1572. 10.1109/TUFFC.2019.2925581 . hal-02195309

HAL Id: hal-02195309

<https://hal.science/hal-02195309v1>

Submitted on 14 Apr 2020

HAL is a multi-disciplinary open access archive for the deposit and dissemination of scientific research documents, whether they are published or not. The documents may come from teaching and research institutions in France or abroad, or from public or private research centers.

L'archive ouverte pluridisciplinaire **HAL**, est destinée au dépôt et à la diffusion de documents scientifiques de niveau recherche, publiés ou non, émanant des établissements d'enseignement et de recherche français ou étrangers, des laboratoires publics ou privés.



Distributed under a Creative Commons Attribution 4.0 International License

Comparison between Multi Line Transmission and Diverging Wave Imaging: assessment of image quality and motion estimation accuracy

Emilia Badescu, Damien Garcia, Philippe Joos, Adeline Bernard, Lionel Augeul, René Ferrera, Magalie Viallon, Lorena Petrusca, Denis Friboulet, Hervé Liebgott

Abstract— High frame rate imaging is particularly important in echocardiography for a better assessment of the cardiac function. Several studies showed that Diverging Wave Imaging (DWI) and Multi Line Transmit (MLT) are promising methods for achieving a high temporal resolution. The aim of this study was to compare MLT and compounded motion compensated (MoCo) DWI for the same transmitted power, the same frame rates (image quality and Speckle Tracking Echocardiography - STE assessment) and the same packet size (Tissue Doppler Imaging – TDI assessment). Our results on static images showed that MLT outperforms DW in terms of resolution (by 30% in average). However, in terms of contrast, MLT outperforms DW only for the depth of 11 cm (by 40% in average), the result being reversed at a depth of 4 cm (by 27 % in average). In vitro results on a spinning phantom at 9 different velocities showed that similar STE axial errors (up to 2.3% difference in median errors and up to 2.1% difference in the interquartile ranges) are obtained with both ultrafast methods. On the other hand, the median lateral STE estimates were up to 13% more accurate with DW than with MLT. On the opposite, the accuracy of TDI was only up to ~3% better with MLT, but the achievable DW Doppler frame rate was up to 20 times higher. However, our overall results showed that the choice of one method relative to the other is therefore dependent on the application. More precisely, in terms of image quality, DW is more suitable for imaging structures at low depths, while MLT can provide an improved image quality at the focal point that can be placed at higher depths. In terms of motion estimation, DW is more suitable for color Doppler related applications, while MLT could be used to estimate velocities along selected lines of the image.

Index Terms— Ultrafast imaging, Diverging waves, Multi Line Transmit, Speckle Tracking, Tissue Doppler Imaging

I. INTRODUCTION

The advantages of echocardiography over other imaging modalities in terms of acquisition time, cost and non-invasiveness justify its common usage in daily clinical practice. Although good clinical results were reported when using the frame rate achievable in standard echocardiography

(~40 to 80 Hz), heart dynamics contains short events that cannot be captured with the conventional frame rate. Higher temporal resolution might be essential in rapid cardiac events observed in a number of cases such as stress echocardiography, fetal echocardiography, multi-chamber motion/strain imaging or intracavitary blood flow dynamics [1]. In response to the need for higher frame rates, several methods have been proposed in ultrasound imaging. The concept of ultrafast echographic imaging was introduced four decades ago by Bruneel *et al.* [2], and this methodology evolved in parallel with the technological progress. Conventionally, an increase in frame rate could be achieved by reducing the line density and/or the sector size, but with the trade-off of resolution loss and field-of-view limitation. To overcome this compromise, a processing method based on reconstructing multiple image lines from one single transmission has been proposed by Shattuck *et al.* [3]. This method is commonly referred to as multi-line-acquisition (MLA) and it is implemented in most current clinical scanners [1]. An alternative technique based on a time reversal approach was introduced by Fink [4]. Other approaches proposed combining images of several subsectors acquired individually at a high frame rate using retrospective electrocardiogram (ECG) gating [5]. A better gain in temporal resolution became possible with the emergence of ultrafast methods which can use both unfocused and focused beams. The unfocused beams approaches use a subaperture to simulate a virtual point located behind the probe. While the first investigations of this approach were referred to as synthetic aperture multi-element techniques [6], later contributions are known as plane (PW) [7] or diverging (DW) [8] waves techniques. As an alternative, the frame rate can be increased using focused beam approaches like multi-line transmission MLT [9]. The achieved high frame rates led to innovative quantitative tools in echocardiography, such as the assessment of the electro-mechanical properties of the heart [10], solving the incompatibility between imaging and quantification for blood flow characterization [11], [12] and the evaluation of 2D vector flow dynamics within the same cardiac cycle [13].

Compared with the conventional single line transmit imaging (SLT), where one focused transmission is needed for each line of the image, MLT principle is based on transmitting n focused beams simultaneously, thus allowing an n -fold increase in frame rate. Several studies based on both

simulations [14] and *in vivo* acquisitions [15] showed the potential of this method in achieving high frame rates while mostly preserving image quality. Additionally, it has been shown that MLT can be efficiently combined with MLA to further improve the temporal resolution. Although the increase in temporal resolution does not compromise to a great extent the contrast, resolution and SNR (signal-to-noise ratio) compared to SLT, it does compromise the amount of image artifacts as a result of simultaneous transmissions. Since MLT is prone to cross-talks, many studies focused on reducing the image artifacts [16], [17], [14]. Although tissue Doppler imaging (TDI) has been applied to MLT images [18], [19] this beamforming method has received little attention in motion estimation.

Alternative ultrafast methods using plane or diverging waves allow one to obtain an entire image with a single transmission. Since the time needed for insonifying a full image by using plane/diverging wave imaging corresponds to the time needed for insonifying n lines of the image with MLT and one single line with SLT, the frame rate is considerably increased. Image quality, however, is significantly compromised in terms of both resolution and contrast [20]. Coherent compounding has thus been proposed to cope with this limitation [6], [20], [21]. By coherently summing multiple images obtained at different PW/DW obliquities, image quality can be improved substantially. Since this approach may fail if the medium is characterized by a strong motion from one transmission to another, motion compensation (MoCo) can be used in the presence of high-velocity tissues to ensure adequate coherent compounding. MoCo was first introduced in synthetic aperture imaging for axial motion compensation [22] and later extended to 2D motion compensation approaches [23]. The potential of MoCo has been shown *in vivo* for abdominal imaging using synthetic aperture approaches [24] and for cardiac imaging using TDI DW approaches [25]. Recently, the importance of using DW MoCo has been demonstrated in improving the STE accuracy [26]. Furthermore, other studies showed that coupling optical flow and TDI methods for STE could provide more precise velocity vector estimates in the in-range direction [27].

In this study, we proposed a comparison between two promising ultrafast methods (DW imaging with MoCo and MLT imaging) in terms of image quality, motion artifacts and their effects on motion estimation using speckle tracking and TDI. To our knowledge, this is the first such comparison proposed in literature.

II. METHODS

A. Acquisition set-up

The data were acquired with a Verasonics research scanner (Verasonics Inc., Redmond, WA) and a P4-2 phased array probe having 64 elements and a central frequency of 2.5 MHz. The pulse repetition frequency (PRF) was set to 4500 Hz, the sector size to 90° and the maximum range to 13 cm.

There are different ways to compare two methods in a fair way. In this study, as a general principle, we have chosen to adapt

the transmission waveform in order to obtain the same total emitted power for both MLT and DW. For MLT, we used an excitation signal which was on during 1/5 of the half cycle and off for the rest of the time. We computed the transmission matrix by overlapping the excitation signals corresponding to all elements and to all simultaneous transmissions. Then, we compared the resulting signals with a threshold in order to obtain a tristate pulse (-1/ 0/ +1) as required by the Verasonics system. The transmitted signal and consequently the transmitted power for MLT were different for each transmission and for each element. However, the total transmitted power calculated over all elements and over all transmissions did not change considerably when the frame rate was varied (the frame rate values will be presented further in sections B and C for speckle tracking and Doppler acquisitions respectively). That was because for a low frame rate, the low power resulted from a reduced superposition of waveforms in a single transmit-event was compensated by summing the power over many transmissions. On the other hand, for a high frame rate, the high power resulted from a high superposition of waveforms in a single transmit-event was compensated by summing the power over less transmissions. But for DW, the total transmitted power decreased with the number of transmissions, since the power in a single event transmission was constant. Therefore, the total transmitted power with MLT did not vary as much with the decrease of the frame rate as it did for DW. We compensated for that by modifying the transmit waveforms when using a reduced number of steering angles for DW. Details about how the excitation signals were changed for DW and about how the power was balanced for static/ STE acquisitions on one hand, and for Doppler acquisitions on the other hand, are provided in sections B and C.

The simulated acoustic pressure field obtained with the two methods for one transmission is represented in Fig. 1.

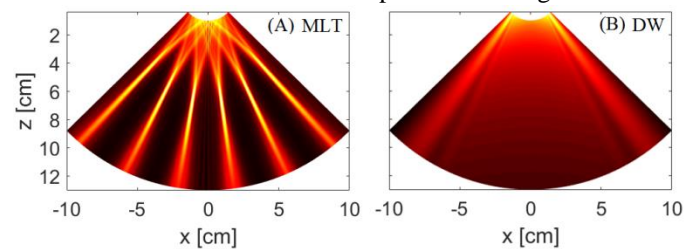


Fig. 1. Pressure field obtained for one transmission with MLT (A) and with DW (B). Results obtained using an in-house simulation tool

B. Acquisition settings for image quality assessment and speckle tracking motion estimator

The same frame rates were used for static conditions and speckle tracking. More specifically, the tested frame rates were set to 225 Hz, 450 Hz and 900 Hz by reducing the number of transmission events per reconstructed image from 20 to 10 and 5. An overview of the transmission setting applied to DW and MLT allowing to obtain the same frame rates is presented in Table I.

The total power of the two high frame-rate methods was balanced using equation 1.

$$P_{MLT/DW}^{BS} = \sum_{t=1}^{N_{tx}} \sum_{e=1}^{N_e} \frac{1}{N_s} \sum_{s=1}^{N_s} |w_{f_{set}}|^2 \quad (1)$$

where $w_{f_{set}}$ represents one sample s of the waveform wf applied to the element e of the transducer for the transmission t ; N_s is the number of samples of the waveform wf , N_e is the number of elements of the transducer and N_{tx} is the total number of transmissions needed to form an image (MLT) or a compound image (DW). This equation holds for both B-mode and STE acquisitions (notation: BS).

Once the power was calculated for each frame rate in MLT, the duty cycle (given by the ratio between the pulse active time and the total period of the pulse) of the transmitted DW waveform was modified to match the same total power for each of the 3 settings. Since the length of the signals was constant (the only parameter changing was the duty cycle), the transmit waveform had half of a cycle for both modalities.

1) Diverging waves

The maximum tilt angle was varied with the number of transmissions. Therefore for the lowest frame rate of 225 Hz, we used the range of $[-8.6^\circ, 8.6^\circ]$, for the frame rate of 450 Hz, we used the range of $[-4.3^\circ, 4.3^\circ]$, and for the highest frame rate of 900 Hz, the maximum tilt angle was $\pm 2.15^\circ$. The resulting lateral (x) positions ranges of the virtual sources obtained using these tilt angle were: $[-2.98, 2.98]$ mm for 20 DW, $[-1.51, 1.51]$ mm for 10 DW and $[-0.75, 0.75]$ mm for 5 DW. Since small maximum tilt angles were employed for all 3 settings, the axial (z) position of the virtual sources slightly changed from -10 mm (tilt angles up to $\pm 4.3^\circ$) to -9.6 mm (tilt angle $\pm 8.6^\circ$). Using a constant angular pitch ensures avoiding transmit grating lobes.

The position of the side lobes changes with the variation of the tilt angles. Even in static conditions, MoCo detects the modification of the side lobes position as a movement. When the tilt angles are linearly increasing, this method rephases the side lobes to the same position. By arranging the tilt angles in a triangular sequence the side lobes can be rephased along two different directions which helps in reducing the side lobes effect [25].

MoCo compensates for the radial motion using the slow time autocorrelation on M successive received IQ signals. The phase angle (ϕ_{MoCo}), giving the phase delays due to motion was calculated using the product of the two autocorrelations (R_1, R_2) corresponding with the ascending and the descending parts of the triangular sequence. As shown in equation 2, a $\frac{1}{2}$ factor is needed to recover the phase angle, which decreases the maximum detectable velocity by a factor 2, compared to the Nyquist velocity.

$$\phi_{MoCo}(\theta, r) = \frac{1}{2} \arg\{R_1 R_2\} \quad (2)$$

where (θ, r) are the polar coordinates and \arg represents the argument of the complex $R_1 R_2$.

The image quality and motion estimation were evaluated on compounded MoCo B-Mode images using the triangular sequence.

2) Multi-Line Transmit

For achieving equivalent temporal resolution, we progressively increased the number of simultaneous transmissions to 3, 6 and 12. The focal point was set to 7 cm. No apodization was used in transmit or receive. Image reconstruction was performed using 5 MLA, meaning that 5 image lines centered in the focal point of the transmitted beam were reconstructed in parallel.

TABLE I
TRANSMISSION SETTINGS MLT VS DW

Frame Rate	Number of Transmit events	MLT: number of simultaneous transmissions	DW: number of tilt angles
225 Hz	20	3	20
450 Hz	10	6	10
900 Hz	5	12	5

C. Acquisition settings for Tissue Doppler Imaging

We fixed constant the two parameters having a high impact on the estimator for both MLT and DW: the PRF and the packet size. Since for DW, the compounding was computed in parallel with the Doppler estimator, the packet size corresponds to the number of tilt angles. Given the PRF of 4500 Hz and a packet size of 8, the resulting Doppler frame rate is 562 Hz. To study the effect of cross-talks in MLT, we kept the same simultaneous focused transmissions configurations as for speckle tracking: 3 MLT, 6 MLT and 12 MLT. However, since we needed to steer 8 times on the same place for each transmission, the Doppler frame rate was drastically decreased to 28 Hz, 56 Hz, 112 Hz. An overview of these parameters is presented in Table II.

TABLE II
TDI TRANSMISSION SETTINGS MLT VS DW

Packet size	MLT		DW	
	Number of simultaneous transmissions	Frame Rate	Number of tilt angles	Frame Rate
8	3	28 Hz	8	562 Hz
8	6	56 Hz	8	562 Hz
8	12	112 Hz	8	562 Hz

For Doppler acquisitions the total power was calculated and balanced using equation 3 for MLT and equation 4 for DW:

$$P_{MLT}^{TDI} = PS \cdot \sum_{t=1}^{N_{tx}} \sum_{e=1}^{N_e} \frac{1}{N_s} \sum_{s=1}^{N_s} |w_{f_{set}}|^2 \quad (3)$$

$$P_{DW}^{TDI} = PS \cdot \sum_{e=1}^{N_e} \frac{1}{N_s} \sum_{s=1}^{N_s} |w_{f_{set}}|^2 \quad (4)$$

where PS is the packet size. We found necessary to use the number of transmissions needed to form a full MLT image, since a 2D autocorrelation was used for Doppler estimation. Therefore, the total power obtained with MLT was much higher than that obtained with DW using half cycle waveforms. Adapting just the duty cycle was not enough to balance the

two total powers. Thus, we needed to use longer waveforms for DW: between 1 and 1.5 cycles for TDI acquisitions, depending on the number of transmissions. Although this allows balancing the total transmitted power, one could expect a direct impact of the pulse length on the TDI performance.

D. In vitro models

1) Image quality assessment on static phantoms

The image quality was firstly evaluated on a Gammex phantom using contrast and resolution metrics as proposed in [28]. Therefore, we used as a metric the Contrast to Noise Ratio (CNR) defined as:

$$CNR = 20 \log_{10} \left(\frac{|\mu_{bck} - \mu_{cyst}|}{\sqrt{\sigma_{bck}^2 + \sigma_{cyst}^2}} \right) \quad (5)$$

where μ_{bck} , μ_{cyst} are the means and σ_{bck}^2 , σ_{cyst}^2 are the corresponding variances of the background and the cyst regions calculated for a B-Mode image.

We evaluated the contrast at 4 cm and 11 cm respectively for the 3 settings mentioned in Table I. Our dynamic range was 60 dB.

For the same acquisition settings, the resolution was evaluated at four different image depths (from 5 cm to 11 cm with a step of 2 cm) using full width at half maximum (FWHM).

2) Image quality assessment on dynamic phantoms

The image quality assessment in dynamic conditions was performed on a tissue mimicking rotating disk phantom made from agar (4%), silica (1%) and water. The disk was created to contain four inclusions for facilitating the contrast assessment (Fig. 3A and B). The CNR was computed using the mean of the four inclusions for each frame. The velocity of the disk was controlled by a step motor and adjusted to 9 different values from 50 %/s to 450 %/s, using a step of 50°.

For each velocity, the mean CNR for the 4 inclusions was averaged over 10 frames.

E. In vivo Models

In vivo data were acquired in an open-chest pig. The experiments were approved by the Animal Ethical Committee with agreement number A693830501. Parasternal short axis views were examined for both B-mode images and tissue Doppler. The acquisition sequences and settings were similar to those used for the in vitro data. The only difference was the focal point for MLT which was placed at 4 cm, due to the available view. The DW and MLT acquisition sequences were concatenated and the buffers were adapted to receive alternatively sets of DW and MLT frames. Thus, the comparison could be assessed at close cardiac phases within the same cardiac cycle. For B-mode images, an intermediate frame rate of 450 Hz was chosen for both DW and MLT (Table I, third row; headings considered as the first row). Similarly, the intermediate settings provided in Table II (third

row; headings considered as the first row) were used for in vivo TDI acquisitions.

F. Motion estimation methods

The influence of the two ultrafast imaging strategies on motion estimation was tested using speckle tracking and tissue Doppler (TDI).

A block matching STE method was used based on the normalized cross correlation in the Fourier domain [29]. The B-Mode images were divided into 32×32 windows. The speckles were tracked with a window overlap of 50%. The pixel size was 0.28 mm in radial direction and 0.3° in the cross range direction. For achieving a subpixel precision parabolic peak fitting was applied to the estimator. Since we used high frame rate imaging, it seemed legitimate to assume constant motion between successive frames. Therefore, to improve the robustness of the method we used an ensemble correlation over 15 frames. The frame lag was increased from 1 to 2 and 4 for the frame rates of 225 Hz, 450 Hz and 900 Hz since it is known that block matching is better adapted to extract displacements greater than one pixel. The speckle tracking parameters (window size, frame lag) were chosen to obtain good estimates when applied to DW images. Then, the same parameters were used for MLT images. Since the two high temporal resolution imaging methods (MLT and DW) were compared at the same frame rates and on images having the same pixel size and number of pixels, choosing the same parameters (frame lag and window size) should provide equivalent conditions for the two methods..

Doppler velocity was estimated using a 2D auto-correlator applied on the IQ data as proposed in [30],[31]. By using this method, the phase shift was used to estimate the displacement. In order to preserve a high Doppler frame rate, TDI was applied to uncompounded DW images. With a PRF of 4500 Hz, the maximum velocity that we could detect with no aliasing was 69 cm/s with MLT and 35 cm/s for DW MoCO (equation 2).

The accuracy of the estimates in a selected direction d was evaluated using the Absolute Deviation Error (ADE) for each pixel i, given by:

$$ADE_{di} = \frac{|V_{ref_{di}} - V_{estim_{di}}|}{|V_{ref_{d}}|_{max}} \quad (6)$$

where $V_{ref_{di}}$, $V_{estim_{di}}$ are the reference and the estimated velocity for a given pixel i and selected direction d (d=x for lateral; d=z for axial); $|V_{ref_{d}}|_{max}$ is the maximum of the absolute reference velocities over the entire image.

III. RESULTS

A. Image quality assessment on static phantoms

Fig. 2 shows the B-Mode images of the Gammex phantom obtained at different frame rates. The left column illustrates the results of using an MLT transmission whereas the right column corresponds to the images resulting from compounded DW. For facilitating the comparison, each row of Fig. 2, displays images acquired at different frame rates.

The contrast values (CNR) for a hypoechoic cyst at 4 cm is reported in Table III and for a cyst at 11 cm in Table IV.

The lateral resolution (FWHM) at 4 different image depths (5 cm, 7 cm, 9 cm, 11 cm) is illustrated in Table V, for all 3

frame rates. However, the resolution did not change significantly from 5 to 10 or 20 DWs. The same trend of lateral resolution saturation starting with a limited number of DWs was also reported in other studies [32].

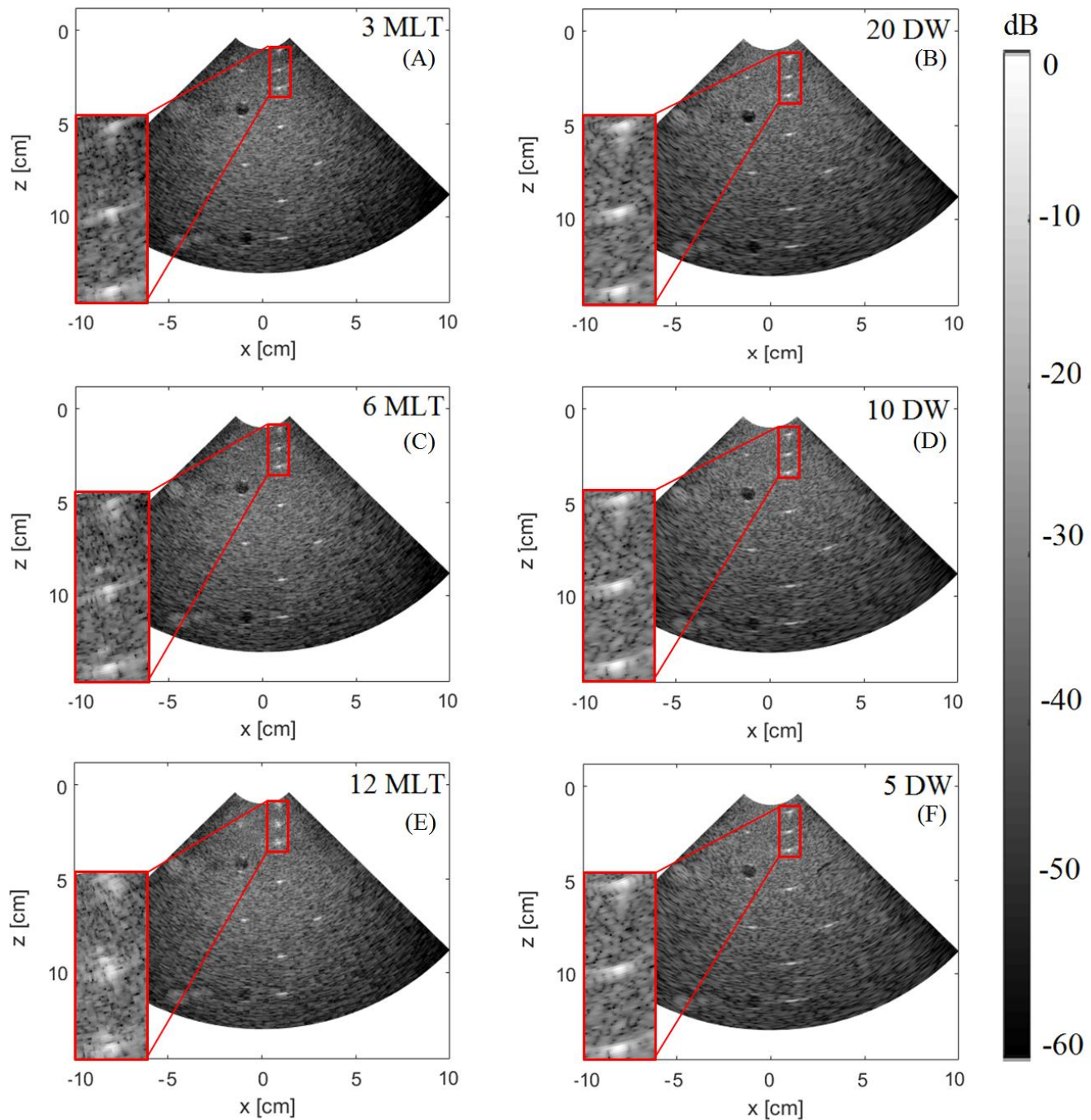


Fig. 2. Image quality for MLT (left column) and DW (right column) by using a frame rate of 225 Hz (A), (B), 450 Hz (C), (D), and 900 Hz (E), (F). A zoomed region ($x=[0.4\text{cm}:1.4\text{cm}]$; $z=[0.8\text{cm}:3.5\text{cm}]$) is provided in the red box for MLT (A, C, E) in comparison with DW (B, D, F) for a better visualization of artifacts next to the surface of the probe.

TABLE III
CNR VALUES FOR CYST AT 4 CM

Frame rate/ Transmission Type	225 Hz	450 Hz	900 Hz
MLT	6.38 dB	5.66 dB	3.75 dB
DW	8.82 dB	7.54 dB	5.36 dB

TABLE IV
CNR VALUES FOR CYST AT 11 CM

Frame rate/ Transmission Type	225 Hz	450 Hz	900 Hz
MLT	5.35 dB	4.46 dB	1.51 dB
DW	4.84 dB	3.53 dB	0.12 dB

TABLE V. LATERAL RESOLUTION AT DIFFERENT IMAGE DEPTHS FOR THE FRAME RATES OF 225 HZ, 450 HZ AND 900 HZ

Transmission Type	Frame rate	225 Hz				450 Hz				900 Hz			
		Depth of the inclusion				Depth of the inclusion				Depth of the inclusion			
		5 cm	7 cm	9 cm	11 cm	5 cm	7 cm	9 cm	11 cm	5 cm	7 cm	9 cm	11 cm
MLT	FWHM	1.6 mm	1.9 mm	2.2 mm	3.6 mm	1.7 mm	1.9 mm	2.2 mm	3.6 mm	1.7 mm	1.9 mm	2.2 mm	3.6 mm
DW		2.1 mm	3.3 mm	3.6 mm	4.5 mm	2.2 mm	3.3 mm	3.6 mm	4.5 mm	2.2 mm	3.3 mm	3.6 mm	4.5 mm

B. Image quality assessment on the rotating disk phantom

In order to observe how the contrast is affected by images undergoing motion, we calculated the CNR for 9 different velocities of the disk. The results are illustrated in Fig. 3. For each velocity we plotted the mean contrast over 10 frames and the corresponding standard deviation.

C. Motion estimation accuracy

Fig. 4 shows the axial (in-range) error distribution while Fig. 5 shows the lateral (cross-range) error distribution using speckle tracking. The median of the ADE is represented in red while the lower and the upper box limit are the first and the third quartiles of the error. The results obtained with MLT (left) and DW (right) at different frame rates are illustrated: 225 Hz (A), (B), 450 Hz (C), (D), 900 Hz (E), (F). Similarly, Fig. 6 shows the TDI results obtained with MLT (left) and DW (right) for the same packet size of 8 and different number of simultaneous transmissions: (A), (C), (E). Below each set of boxplots we show the differences in median (*Med*) and interquartile range (*IQR*) between MLT and DW. The *IQR*

was calculated by subtracting the 25th percentile from the 75th percentile of the ADE. In order to study if the medians and *IQRs* obtained with the two methods are statistically different, we used a two-sided Wilcoxon rank sum test between the 2 groups (MLT and DW) containing 9 samples each (one for each velocity). The last column from each table shows if the resulting p-value allows rejecting the null-hypothesis at 5% significance level.

D. Qualitative B-mode and TDI in vivo assessment

In Fig. 7, we show B-mode images obtained at the intermediate frame rate of 450 Hz for both MLT (A) and DW (B). Additionally, we show in Fig. 8 the tissue Doppler images for the two high frame rate methods. Two pairs of TDI images are shown at two different phases of the cardiac cycles. MLT and DW TDI results are firstly shown during ventricular filling when the mitral valve is fully opened (A,B) and secondly the same images are shown when the mitral valve starts to close (C,D).

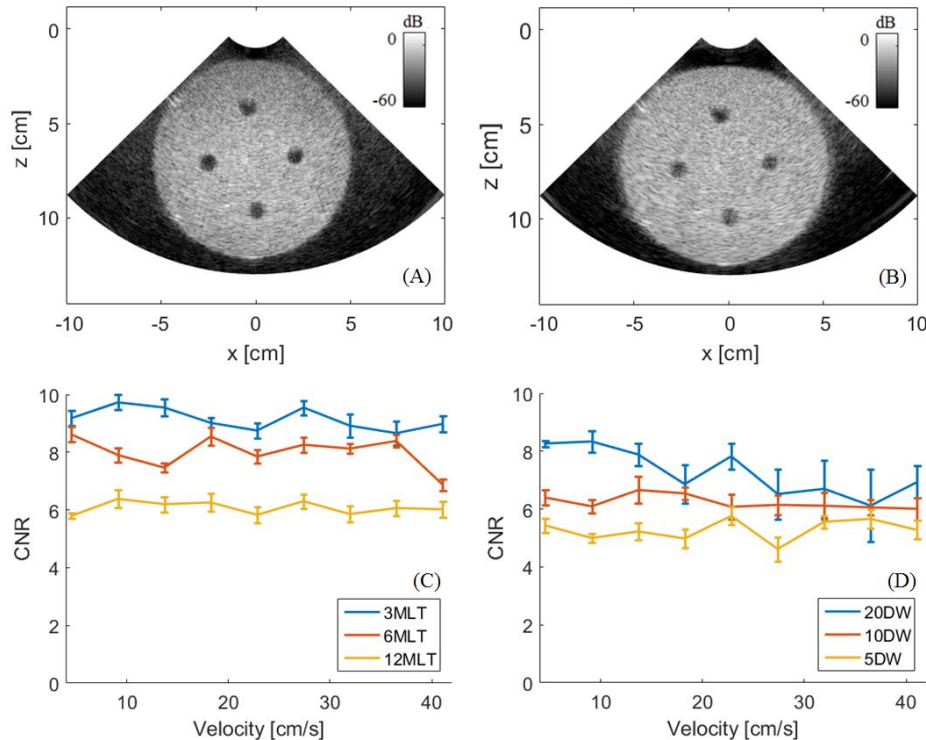


Fig. 3. CNR at different velocities of the disk calculated on the phantom showed (for qualitative evaluation) in (A) for MLT and in (B) for DW. Results for MLT (C) and DW (D) at a frame rate of 225 Hz (blue), 450 Hz (red) and 900 Hz (yellow)

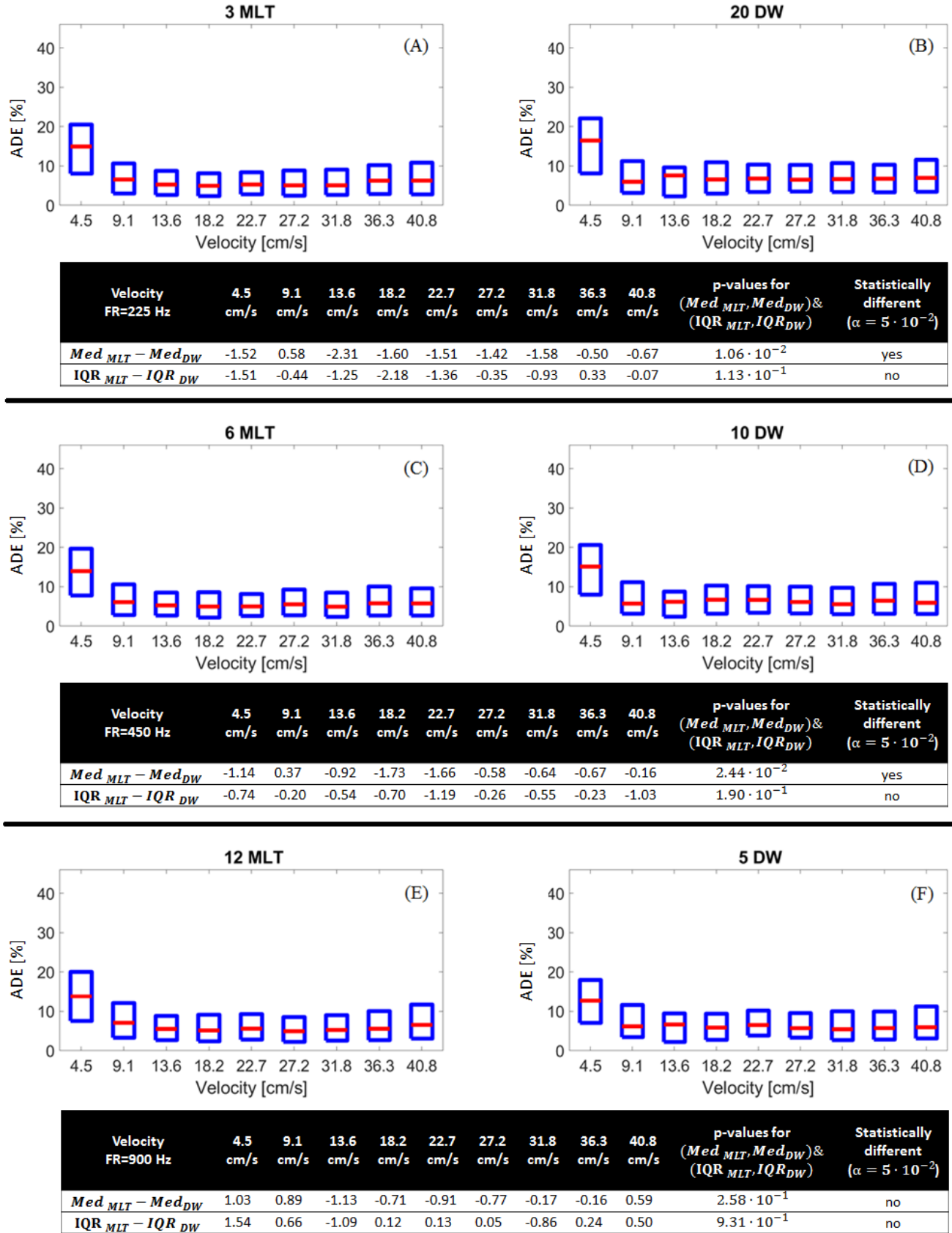


Fig. 4. Axial ADE at different velocities of the disk at different frame rates (Speckle Tracking): 225 Hz (A), (B); 450 Hz (C), (D) and 900 Hz (E), (F). Below each set of boxplots we show the differences in median (Med) and interquartile range (IQR) between MLT and DW. Additionally, we provide the associated p-values.

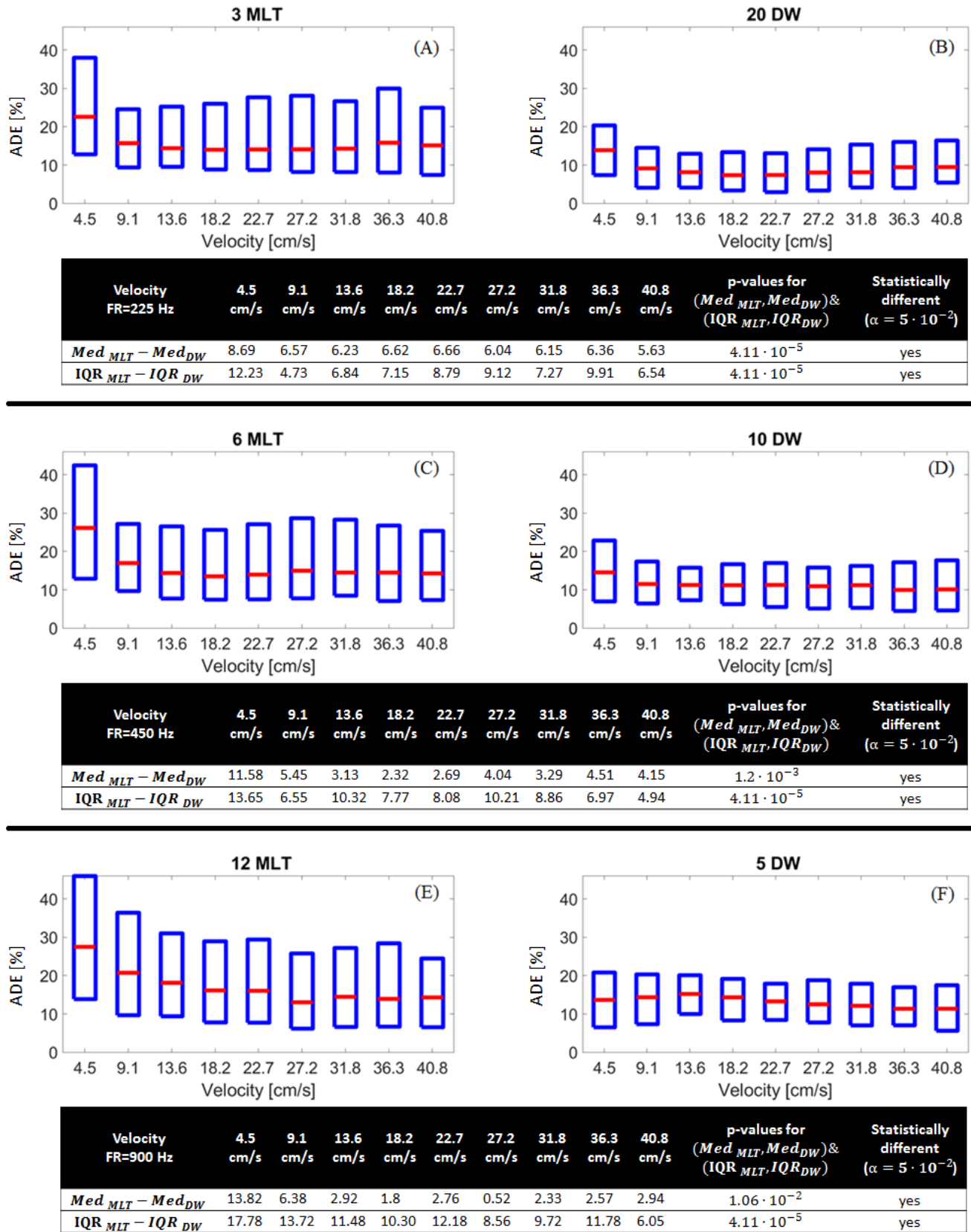


Fig. 5. Lateral (right) ADE at different velocities of the disk at different frame rates (**Speckle Tracking**): 225 Hz (A), (B); 450 Hz (C), (D) and 900 Hz (E), (F). Below each set of boxplots we show the differences in median (Med) and interquartile range (IQR) between MLT and DW. Additionally, we provide the associated p-values.

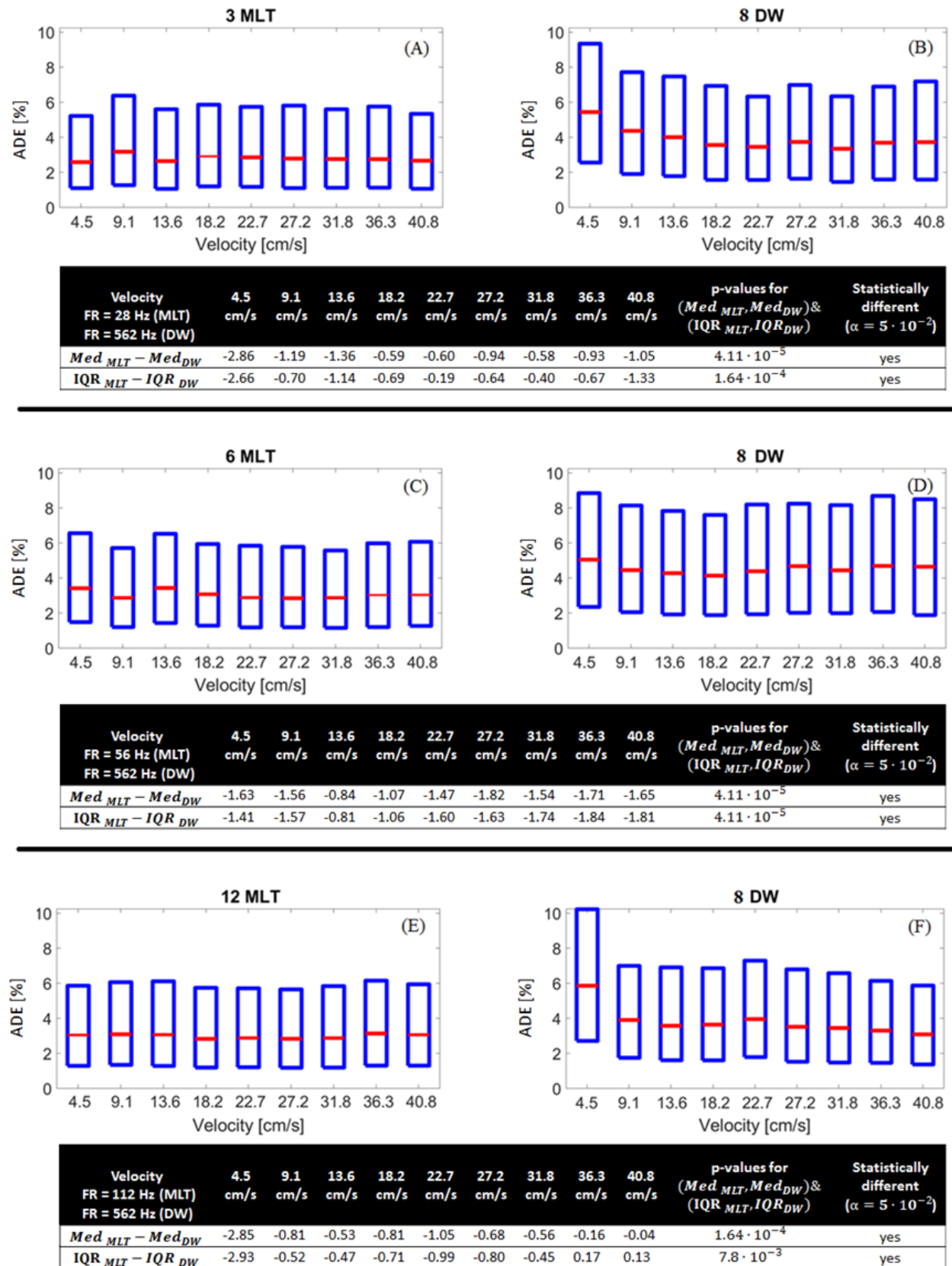


Fig. 6. Axial ADE at different velocities of the disk (Doppler) by fixing the packet size to 8. The transmitted power was adjusted for DW to compare (A) with (B), (C) with (D) and (E) with (F). Below each set of boxplots we show the differences in median (Med) and interquartile range (IQR) between MLT and DW. Additionally, we provide the associated p-values.

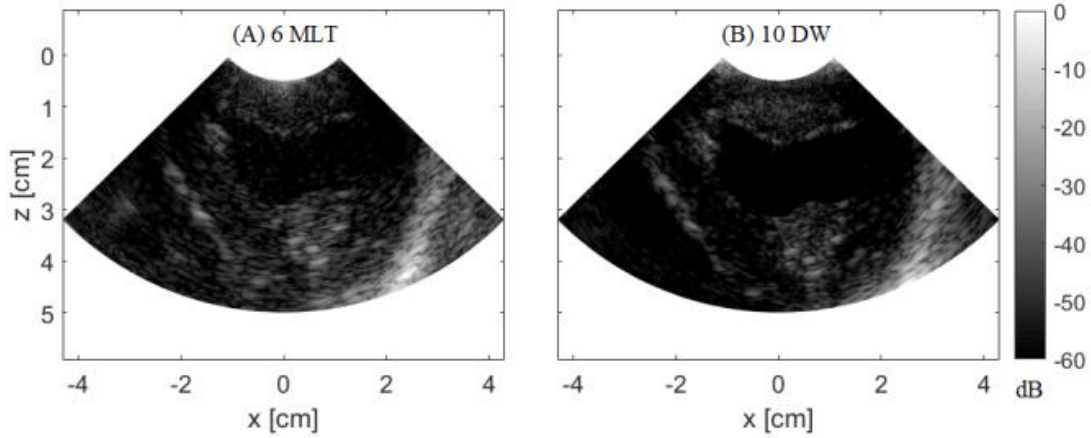


Fig. 7. B-mode in vivo images for MLT (A) and DW (B) at a frame rate of 450 Hz for the same phase of the cardiac cycle

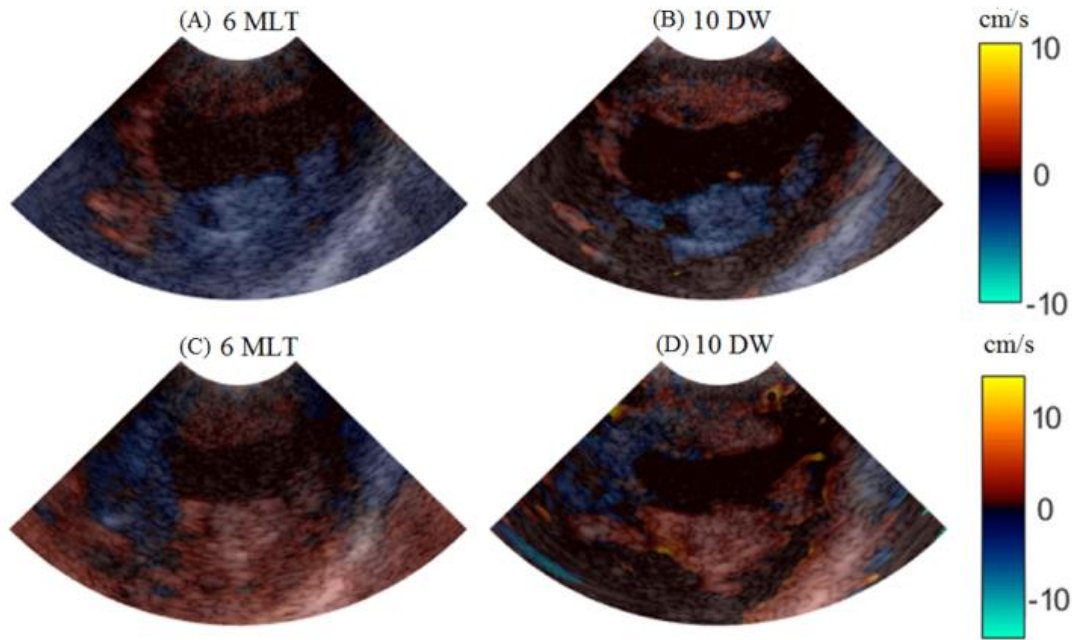


Fig. 8. TDI in vivo images for MLT (A,C) and DW (B,D) during two phases of the cardiac cycle: when the mitral valve is fully opened (A,B) and when the mitral valve starts to close (C,D).

IV. DISCUSSION

A. Image quality assessment: phantom experiments

Fig. 2 shows the image quality degradation with the decrease of the number of transmissions and therefore the increase in frame rate. Even if the degradation was present for both MLT and DW its nature was different for the two methods. For instance, for MLT, the amount of cross talk artifacts at a depth up to 4 cm was considerably increased as seen in magnified regions marked by the red boxes of Fig. 2 (A), Fig. 2 (C) and Fig. 2 (E). On the other hand, using DW led to a good image quality up to 4 cm. In addition to the absence of cross-talks, the CNR of the cyst placed at 4 cm was higher for the DW wide beam transmission as compared to the focused beam transmission (Table III). However, DW showed a higher attenuation of the signal at higher depths compared to MLT for all frame rates (although the transmitted energy was equivalent for the two methods). This explains the CNR values for the

cyst at 11 cm that were reduced when the unfocused DW transmission was used compared to MLT (Table IV). This phenomenon appears even though the position of the cyst at 11 cm is 4 cm away from the focal point.

We evaluated the lateral resolution starting from 5 cm to 11 cm with a step of 2 cm. Our results (Table V) showed that similar FWHM values are obtained for the same depth and a different frame rate, which is consistent with other studies from the literature, showing that the lateral resolution improves quickly with the number of diverging waves [32]. Moreover, for all settings considered, we were above 3 diverging waves, which is the value required for stabilizing the lateral resolution. As it can be observed in Table V, a better resolution was achieved by using MLT than by using DW and the resolution degraded with depth for both methods. However, the lateral resolution with DWI could be improved further by using a higher angular pitch.

The qualitative contrast evaluation on the rotating disk phantom showed in Fig. 3 A and B indicates the trend of MLT to offer a better contrast for the inclusions close to the

focal point and the trend of DW to offer a better contrast at low depths. The quantitative assessment over all inclusions showed the degradation of the contrast with the increase of the temporal resolution for all the velocities applied to the motor (Fig. 3 C and D). Note that the higher CNR values obtained in the rotating disk phantom compared with the Gammex phantom came from the difference in echogenicity between the two phantoms. The CNR was approximately constant with the variation of the velocity, which is consistent with the results presented in [25]. However, the curves present slight deviations which appeared as a consequence of calculating the average CNR at different positions of the inclusions at different velocities. Despite this limitation, the trend of a better MLT contrast compared to DW MoCo can still be observed for all velocities and for all frame rates. This can be explained by the fact that the cysts were placed from 4.5 cm to 9.5 cm in a region of interest where we showed that MLT is likely to be more accurate. Evaluating the CNR in dynamic conditions at lower penetration depths may lead to opposite results since the MLT cross-talks level is increased at low depths.

B. Motion estimation assessment: phantom experiments

When speckle tracking was applied to MLT images and compounded motion-compensated DW images, similar medians and IQR values were obtained in both cases in the axial direction for each frame rate and velocity value (Fig. 4). For all the acquisitions, the difference in median and IQR was inferior to 2.3%. The predominant negative values for the frame rates of 225 Hz and 450 Hz show the trend of MLT to perform slightly better than DW, which can be associated with the impact of focusing on the B-Mode image quality. On the other hand, this trend is less general for the frame rate of 900 Hz where the presence of transmit artifacts in MLT is more significant. Despite the small differences (less than 2.3 %) in medians for the frame rates of 225 Hz and 450 Hz, the p-value shows that the two methods provide statistically different medians of error. This can be explained by the fact that each median is calculated over a very large number of samples ($\sim 10^7$), resulting in narrow and non-overlapping distributions of each two groups tested.

The difference between the results obtained with the two methods is larger in the lateral direction especially in terms of interquartile range, going up to 17.7 % (Fig. 5). The p-values reported in Fig. 5 show that the difference in results between the two methods is statistically significant for all frame rates and for both IQR and medians. The lower performance of MLT can be associated with the discontinuities between the lines of the images found on the B-Mode images. The image appearance looks smoothed in DW compared to MLT due to the compounding process. Additionally, the lateral performance could be improved by reducing the cross-talk level as suggested in [15]. For both directions and all frame rates considered, we can observe the trend of the block matching to provide less accurate

estimates at the lowest velocity (reduced movement between the frames). Since we compensated for a higher temporal resolution by incrementing the lag between the frames, the estimator is not significantly affected by the frame rate variation.

When TDI was investigated for the two high-frame rate methods, the predominant negative difference in medians and IQR indicates slightly better estimates for MLT (Fig. 6). However, the improvement was inferior to 3% for all the cases. On the other hand, DW allows performing compounding and MoCo for B-Mode visualization based on the same packet size used for motion estimation. Thus the temporal resolution is diminished just by a single parameter: the packet size. On the opposite, for estimating the Doppler velocities on MLT images while preserving a high PRF, successive transmissions have to be performed several times for the same image location. Therefore, the time required between the formation of the first and the last line of the image is increased not just with the packet size but also with the number of transmissions needed to achieve a full B-Mode image. In consequence, the Doppler frame rate is significantly limited as compared to a DW transmission. As shown in Table II, this leads to frame rates of 28 Hz, 56 Hz and 112 Hz, depending on the amount of cross talks we would be ready to accept, as compared to a frame rate of 562 Hz with DW. Using a higher number of steering angles in DW may improve the Doppler estimates, while providing a high enough frame rate, but increasing the packet size in MLT would reduce drastically the Doppler temporal resolution. For instance, using 32 steering angles for the first will result in a Doppler frame rate of 140 Hz whereas using a 32 packet size for 3 MLT will result in a Doppler frame rate of 7 Hz. Additionally, an overlap of 50 % can be used for the DW transmissions as suggested in [25], which would allow frame rates twice higher. If the two methods had been compared at the same Doppler frame rates, it is very likely that DW would have performed better than MLT. Using a higher number of transmissions for MoCo would have resulted in a better synthetic focusing. However, it would have been difficult to assess if the performance of the DW Doppler estimator had come from decreased variance (as a result of the packet size increase) or from the inherent features of the data obtained with the two imaging modalities (MLT and DW).

By increasing the number of cycles from 1 and 1.5 cycles in TDI (to balance the total power from 6 MLT to 3 MLT configurations), the TDI accuracy is influenced. For instance, we can observe a slight difference in the median ADE between Fig. 6 B and Fig. 6 D, which in average (over all velocities) is 13%.

A possible improvement of the TDI estimator for both methods could have been achieved by using even longer transmission pulses (more cycles). However, due to hardware constraints, we could not increase the duration of the transmitted MLT signal and we needed to balance the DW transmission signal accordingly (equations 3-4). It is also worth mentioning that balancing the total power of the transmitted waveforms does not guarantee the same

acoustic power for the two methods, which could be an alternative to our acquisition settings.

C. *In-vivo acquisitions*

B-mode *in vivo* acquisitions showed that the two methods are competitive in providing good image quality at high frame rates (Fig. 7). However, the presence of cross-talks next to the surface of the probe in MLT makes DW a better candidate for the visualization of low depth structures. This could explain the cluttered appearance of MLT images. The presence of these artifacts in the region of interest could be reduced by placing a gel pad between the probe and the surface of the heart. As also demonstrated *in vitro*, the contrast up to 4 cm is better with DW than with MLT. TDI images illustrated in Fig. 8 demonstrate competitive performances of the two methods in providing good qualitative velocity estimates.

D. *Overall results and limitations*

Overall, the obtained results show that the choice of using one ultrafast method over the other depends on the application. Even if for the B-Mode visualization of organs placed at a lower depth, DW is more adapted than MLT, the energy dissipates faster with the penetration depth compared to MLT. Although cardiac images are characterized by rapid movements, the CNR seem to be better preserved with MLT. Competitive speckle tracking estimates were found for the two methods in the axial direction, while the error was significantly higher for MLT in the lateral direction. In terms of Doppler velocity estimator, MLT provides slightly lower errors than DW, but much higher Doppler frame rates can be obtained with DW. Even if MLT may be enough for TDI, higher frame rate may be desirable for blood velocity estimation, case in which DW would be more adapted. Since the MLT Doppler temporal resolution is considerably affected if a full image needs to be reconstructed, estimating the velocity just over a few lines of interest in the image would definitely eliminate this limitation.

It is important to highlight that our overall results are valid for our specific acquisition settings that were fixed to provide similar conditions for the two methods (same transmitted power, frame rate for image quality and STE and same packet size for TDI). An interesting alternative to our choice would have been to optimize each method. Using coded excitations could have been an interesting approach. Due to hardware constraints, we could not use a longer pulse for MLT and we adapted the transmitted signal for DW accordingly. Moreover, comparing the two methods at the same frame rate for TDI would have resulted in superior performances of DWI.

V. CONCLUSION

In this study, we compared two ultrafast methods in static and dynamic conditions for *in vitro* and *in vivo* experiments.

Since both methods can provide competitive frame rates compared to conventional imaging, our aim was to evaluate their performance at different frame rates, superior to the ones specific for SLT. We were particularly interested in analyzing the image quality and in assessing the influence of each ultrafast method on two motion estimation techniques commonly used in echocardiography: speckle tracking and tissue Doppler imaging.

The performance of the two ultrafast competitive methods was investigated for different frame rates and different velocities. DW imaging provides better image quality at limited depths whereas MLT imaging allows a better concentration of the energy around a focal point that could be placed at higher depths. Similar speckle tracking axial errors were obtained for the two methods, but DW with MoCo provides better lateral estimates than MLT. Slightly lower TDI errors were obtained for MLT but much higher Doppler frame rates can be obtained with DW.

The two methods showed to be competitive in both image quality and motion estimation and the choice for a certain method is dependent on the application.

For example, DWI is more suitable for color Doppler applications due to the high frame rate that could be achieved by using this imaging method. Also, imaging structures at low depth at good image quality and without any particular artifacts (as it would be the case for MLT) can definitively be obtained with DW. On the other hand, MLT can provide very good image quality close to the focal point (that could be placed at higher depths) and time-resolved velocities along different lines of the image (corresponding to simultaneous transmissions).

ACKNOWLEDGMENT

This project has received funding from the European Union's Horizon 2020 research and innovation programme under the Marie Skłodowska-Curie grant agreement No 642612, VPH-CaSE (www.vph-case.eu). This work was performed within the framework of the LABEX PRIMES (ANR-11-LABX-0063) of Université de Lyon, within the program "Investissements d'Avenir" (ANR-11-IDEX-0007) operated by the French National Research Agency (ANR). This work was also supported by LABEX CELYA (ANR-10-LABX-0060).

The Verasonics system was cofounded by the FEDER program, Saint-EtienneMetropole (SME) and Conseil General de la Loire (CG42) within the framework of the SonoCardioProtection Project led by Dr Pierre Croisille.

REFERENCES

- [1] M. Cikes, L. Tong, G. R. Sutherland, and J. D'hooge, "Ultrafast Cardiac Ultrasound Imaging," *JACC Cardiovasc. Imaging*, vol. 7, no. 8, pp. 812–823, Aug. 2014.
- [2] C. Bruneel, R. Torguet, K. M. Rouvaen, E. Bridoux, and B. Nongaillard, "Ultrafast echotomographic system using optical processing of ultrasonic signals," *Appl. Phys. Lett.*, vol. 30, no. 8, pp. 371–373, Apr. 1977.
- [3] D. P. Shattuck, M. D. Weinschenker, S. W. Smith, and O. T. von Ramm, "Explosocan: A parallel processing technique for high speed ultrasound imaging with linear phased arrays," *J. Acoust. Soc. Am.*, vol. 75, no. 4, pp. 1273–1282, Apr. 1984.
- [4] M. Fink, "Time reversal of ultrasonic fields. I. Basic principles," *IEEE Trans. Ultrason. Ferroelectr. Freq. Control*, vol. 39, no. 5, pp. 555–566, Sep. 1992.
- [5] Shougang Wang, Wei-ning Lee, J. Provost, Jianwen Luo, and E. E. Konofagou, "A composite high-frame-rate system for clinical cardiovascular imaging," *IEEE Trans. Ultrason. Ferroelectr. Freq. Control*, vol. 55, no. 10, pp. 2221–2233, Oct. 2008.
- [6] M. Karaman, Pai-Chi Li, and M. O'Donnell, "Synthetic aperture imaging for small scale systems," *IEEE Trans. Ultrason. Ferroelectr. Freq. Control*, vol. 42, no. 3, pp. 429–442, May 1995.
- [7] L. Sandrin, S. Catheline, M. Tanter, X. Hennequin, and M. Fink, "Time-Resolved Pulsed Elastography with Ultrafast Ultrasonic Imaging," *Ultrason. Imaging*, vol. 21, no. 4, pp. 259–272, Oct. 1999.
- [8] H. Hasegawa and H. Kanai, "High-frame-rate echocardiography using diverging transmit beams and parallel receive beamforming," *J. Med. Ultrason.*, vol. 38, no. 3, pp. 129–140, Jul. 2011.
- [9] R. Mallart and M. Fink, "Improved imaging rate through simultaneous transmission of several ultrasound beams," 1992, pp. 120–130.
- [10] J. Provost, Wei-Ning Lee, K. Fujikura, and E. E. Konofagou, "Electromechanical Wave Imaging of Normal and Ischemic Hearts In Vivo," *IEEE Trans. Med. Imaging*, vol. 29, no. 3, pp. 625–635, Mar. 2010.
- [11] S. I. Nikolov and J. A. Jensen, "In-vivo synthetic aperture flow imaging in medical ultrasound," *IEEE Trans. Ultrason. Ferroelectr. Freq. Control*, vol. 50, no. 7, pp. 848–856, Jul. 2003.
- [12] C. Papadacci, M. Pernot, M. Couade, M. Fink, and M. Tanter, "High-contrast ultrafast imaging of the heart," *IEEE Trans. Ultrason. Ferroelectr. Freq. Control*, vol. 61, no. 2, pp. 288–301, Feb. 2014.
- [13] J. Faurie *et al.*, "Intracardiac Vortex Dynamics by High-Frame-Rate Doppler Vortography—In Vivo Comparison With Vector Flow Mapping and 4-D Flow MRI," *IEEE Trans. Ultrason. Ferroelectr. Freq. Control*, vol. 64, no. 2, pp. 424–432, Feb. 2017.
- [14] L. Tong, H. Gao, and J. D'hooge, "Multi-transmit beam forming for fast cardiac imaging—a simulation study," *IEEE Trans. Ultrason. Ferroelectr. Freq. Control*, vol. 60, no. 8, pp. 1719–1731, Aug. 2013.
- [15] L. Tong, A. Ramalli, R. Jasaityte, P. Tortoli, and J. D'hooge, "Multi-Transmit Beam Forming for Fast Cardiac Imaging - Experimental Validation and In Vivo Application," *IEEE Trans. Med. Imaging*, vol. 33, no. 6, pp. 1205–1219, Jun. 2014.
- [16] L. Demi, M. D. Verweij, and K. W. A. Van Dongen, "Parallel transmit beamforming using orthogonal frequency division multiplexing applied to harmonic imaging—A feasibility study," *IEEE Trans. Ultrason. Ferroelectr. Freq. Control*, vol. 59, no. 11, pp. 2439–47, Nov. 2012.
- [17] A. Rabinovich, A. Feuer, and Z. Friedman, "Multi-line transmission combined with minimum variance beamforming in medical ultrasound imaging," *IEEE Trans. Ultrason. Ferroelectr. Freq. Control*, vol. 62, no. 5, pp. 814–827, May 2015.
- [18] L. Tong *et al.*, "Wide-Angle Tissue Doppler Imaging at High Frame Rate Using Multi-Line Transmit Beamforming: An Experimental Validation In Vivo," *IEEE Trans. Med. Imaging*, vol. 35, no. 2, pp. 521–528, Feb. 2016.
- [19] A. Ramalli *et al.*, "Real-Time High-Frame-Rate Cardiac B-Mode and Tissue Doppler Imaging Based on Multiline Transmission and Multiline Acquisition," *IEEE Trans. Ultrason. Ferroelectr. Freq. Control*, vol. 65, no. 11, pp. 2030–2041, Nov. 2018.
- [20] G. Montaldo, M. Tanter, J. Bercoff, N. Benech, and M. Fink, "Coherent plane-wave compounding for very high frame rate ultrasonography and transient elastography," *IEEE Trans. Ultrason. Ferroelectr. Freq. Control*, vol. 56, no. 3, pp. 489–506, Mar. 2009.
- [21] C. Papadacci, M. Pernot, M. Couade, M. Fink, and M. Tanter, "High-contrast ultrafast imaging of the heart," *IEEE Trans. Ultrason. Ferroelectr. Freq. Control*, vol. 61, no. 2, pp. 288–301, Feb. 2014.
- [22] G. E. Trahey and L. F. Nock, "Synthetic receive aperture imaging with phase correction for motion and for tissue inhomogeneities. II. Effects of and correction for motion," *IEEE Trans. Ultrason. Ferroelectr. Freq. Control*, vol. 39, no. 4, pp. 496–501, Jul. 1992.
- [23] B. Denarie *et al.*, "Coherent Plane Wave Compounding for Very High Frame Rate Ultrasonography of Rapidly Moving Targets," *IEEE Trans. Med. Imaging*, vol. 32, no. 7, pp. 1265–1276, Jul. 2013.
- [24] K. L. Gammelmark and J. A. Jensen, "2-D tissue motion compensation of synthetic transmit aperture images," *IEEE Trans. Ultrason. Ferroelectr. Freq. Control*, vol. 61, no. 4, pp. 594–610, Apr. 2014.
- [25] J. Poree, D. Posada, A. Hodzic, F. Tournoux, G. Cloutier, and D. Garcia, "High-Frame-Rate Echocardiography Using Coherent Compounding With Doppler-Based Motion-Compensation," *IEEE Trans. Med. Imaging*, vol. 35, no. 7, pp. 1647–1657, Jul. 2016.
- [26] P. Joos *et al.*, "High-Frame-Rate Speckle-Tracking Echocardiography," *IEEE Trans. Ultrason. Ferroelectr. Freq. Control*, vol. 65, no. 5, pp. 720–728, May 2018.
- [27] J. Poree, M. Baudet, F. Tournoux, G. Cloutier, and D. Garcia, "A Dual Tissue-Doppler Optical-Flow Method for Speckle Tracking Echocardiography at High Frame Rate," *IEEE Trans. Med. Imaging*, vol. 37, no. 9, pp. 2022–2032, Sep. 2018.
- [28] H. Liebgott, A. Rodriguez-Molares, F. Cervenansky, J. A. Jensen, and O. Bernard, "Plane-Wave Imaging Challenge in Medical Ultrasound," in *2016 IEEE International Ultrasonics Symposium (IUS)*, 2016, pp. 1–4.
- [29] I. A. Hein and W. D. O'Brien, "Current time-domain methods for assessing tissue motion by analysis from reflected ultrasound echoes—a review," *IEEE Trans. Ultrason. Ferroelectr. Freq. Control*, vol. 40, no. 2, pp. 84–102, Mar. 1993.
- [30] C. Kasai, K. Namekawa, A. Koyano, and R. Omoto, "Real-Time Two-Dimensional Blood Flow Imaging Using an Autocorrelation Technique," *IEEE Trans. Sonics Ultrason.*, vol. 32, no. 3, pp. 458–464, May 1985.
- [31] T. Loupas, J. T. Powers, and R. W. Gill, "An axial velocity estimator for ultrasound blood flow imaging, based on a full evaluation of the Doppler equation by means of a two-dimensional autocorrelation approach," *IEEE Trans. Ultrason. Ferroelectr. Freq. Control*, vol. 42, no. 4, pp. 672–688, Jul. 1995.
- [32] M. Zhang *et al.*, "Extension of Fourier-Based Techniques for Ultrafast Imaging in Ultrasound With Diverging Waves," *IEEE Trans. Ultrason. Ferroelectr. Freq. Control*, vol. 63, no. 12, pp. 2125–2137, Dec. 2016.